IEEE Access
Multidisciplinary | Rapid Review | Open Access Journal

Received October 19, 2019, accepted October 30, 2019, date of publication November 4, 2019, date of current version November 21, 2019.

Digital Object Identifier 10.1109/ACCESS.2019.2951170

The Attitude Control Algorithm of Agile Optical Satellite Oriented to Nonparallel-Ground-Track-Imaging

LIN ZHAO, KUN ZHAO, YONG HAO, XINYU ZHANG, AND YUSHAN HE
Automation College, Harbin Engineering University, Harbin 150001, China

Corresponding author: Yong Hao (haoyong@hrbeu.edu.cn)

This work was supported in part by the National Natural Science Foundation of China under Grant 61633008, and in part by the Natural Science Foundation of Heilongjiang Province, China, under Grant F2017015.

ABSTRACT This paper concerns the control algorithm oriented to nonparallel-ground-track-imaging for agile optical satellite. Firstly, for obtaining the desired trajectory, the mapping relationship between the satellite attitude and the ground stripe is established by using space vector method. According to the mapping function, an attitude adjustment strategy via constant scanning velocity is proposed. Then, considering the exact information of the external disturbance cannot be obtained and the input saturation problem, a robust anti-saturation tracking controller is designed via fixed-time disturbance observer and integral sliding mode. Finally, the effectiveness of the proposed control algorithm is illustrated by numerical simulation.

INDEX TERMS Agile optical satellite, nonparallel-ground-track-imaging, integral sliding mode, disturbance observer, input saturation.

I. INTRODUCTION

With further development of the space remote sensing technology, the requirement for earth observation is becoming more and more complex. Agile optical satellite (AOS) has the characteristics of rapid attitude maneuver, thereby being widely applied for the earth observation missions [1]–[3]. Compared with general optical satellite, AOS can observe the ground targets continuously while maneuvering, which means it can coverage wider area and observe more quantities of potential targets within a finite observation interval.

Nonparallel-Ground-Track-Imaging (NGTI) is a complex imaging mode oriented to the ground trajectory which is not parallel to the sub-satellite line [4]. NGTI has a better effect on the irregular narrow observation areas, such as the borderline, the coastline and the seismic belt. Due to imaging for the ground target dynamically and continuously, the satellite attitude should be well controlled. To this end, tremendous control methods were applied in the last decades, involving the backstepping control [5], [6], the neural-network control [7]–[11], the adaptive control [12], [13], the event-triggered control [14], [15] and the sliding mode control [16]–[19].

The associate editor coordinating the review of this manuscript and approving it for publication was Xiwang Dong.

The external disturbance is an important factor that affects the satellite control quality thereby affecting the imagery quality. Controllers developed in a lot of literatures were effective to solve the control problem on condition that the exact information of the external disturbance has been given, however, this situation is not always met. As a result, manifold adaptive control strategies are established to estimate and compensate the uncertain time-varying disturbances [5]–[14]. In [5], almost globally fixed-time stabilization could be obtained via the fuzzy logic based backstepping attitude tracking control method even under complex external disturbances. As for a single flexible spacecraft, it gave an ideal solution by virtue of the Chebyshev neural network in [10], which can reconfigure the control system as external disturbances and internal parameters vary. Considering the wide application of spacecraft formation flying (SFF), backstepping control methods incorporating the second-order sliding mode differentiator and command filter was exploited in [6]. Analogously for the leader-follower satellite formation task, the reconfiguration algorithm in [11] is developed on the basis of neural network, where the finite-time stability could be ensured. Different from the leader follower formation structure, the distributed formation strategies also play a significant role due to the advantages of its flexibility and

fault-tolerant ability. Thus, an attitude coordination control framework was employed in [7] by utilizing the Chebyshev neural networks to compensate the time-varying reference. Furthermore, the modified fast terminal sliding mode has been applied when there existed system parameter uncertainties and input saturation constraints [8]. However, the unit quaternion based attitude description in [7], [8] is the main cause for the unwinding phenomenon, which will lead to unnecessary fuel consumption. Fortunately, rotation matrix is the other alternative for attitude description, which will deal with the unwinding problem properly.

The disturbance observer, which is famous due to its precise estimation for disturbances, has also been widely researched in aerospace engineering [20]–[25]. In [20], the robustness of the spacecraft attitude control system is significantly enhanced by resorting to a specially designed disturbance observer, which can effectively estimate the external disturbance. As a further technological extension, two disturbance observers have been established in [17] and [21] such that the formation task could be accomplished under seriously disturbed environment. Considering for the convergence rate, controllers proposed in [21]–[25] possess finite-time stability. Especially, methods in [23] is capable of tackling the actuator fault and the input saturation constraint will not be violated in [24], [25].

As a matter of fact, input saturation constraints must be carefully taken into account during the attitude controller design process, otherwise control system performance will degrade severely. In real applications, input saturation constraint is mainly caused by the physical constraints of the mechanical components. In [26], Liu *et al.* conducted a special exploration on the issue of actuator saturation and deduced a sample state feedback controller, which tackled the input magnitude and rate constraints via the linear matrix inequality method. In [27], the devised control scheme possesses good robustness against the actuator fault and input saturation constraints. Though effective, the proposed methods mentioned above cannot satisfy a prescribed performance introduced by designers, which will be well solved in [28].

It should be noted that if the ground trajectory is expected to be tracked exactly by the optical camera, a desired satellite attitude must be given in advance, that means, a mapping relationship should be firstly established between the ground trajectory and the satellite attitude. However, there is little research on this aspect. Generally, tracking the ground trajectory can be realized by merely adjusting the roll-axis and pitch-axis of the satellite, however, due to the impact of earth's rotation, orbital motion and attitude maneuvering, a drift angle is usually generated which will affect the image quantity [29]. In [4], Ye *et al.* proposed a strategy to eliminate the drift angle by adjusting the yaw-axis, however, the deduction was not accurate enough.

In summary, the attitude adjustment and control oriented to NGTI for the AOS is still a challenging problem. Inspired by the observation summarized above, this paper proposes an attitude control algorithm oriented to NGTI. To be specific, the contribution of this paper can be given as follows:

i) A mapping function between the satellite attitude and the ground trajectory is established by using space vector method. On this basis, an attitude adjustment strategy via constant scanning velocity is proposed.

ii) A fixed-time disturbance observer is designed based on the Gudermannian equation. It is noteworthy that the disturbance observers in [17]–[19] were asymptotically stable. Compared with [17]–[19], the convergence time of the proposed observer could be regulated according to system demands.

iii) Different from the existing anti-saturation methods in [26]–[28], an anti-saturation robust tracking controller via integral sliding mode method is designed in this paper, which is derived on the basis of the property of hyperbolic tangent function and Eulerian-Lagrangian system.

The remainder of this paper is given as follows. In section II, problem description and modelling are presented. In section III, satellite attitude adjustment strategy for NGTI is proposed. Section IV is devoted to controller design and stability analysis. In section V, numerical simulations are conducted to show the effectiveness of the proposed algorithm. Finally, it comes to the conclusion of this paper in section IV.

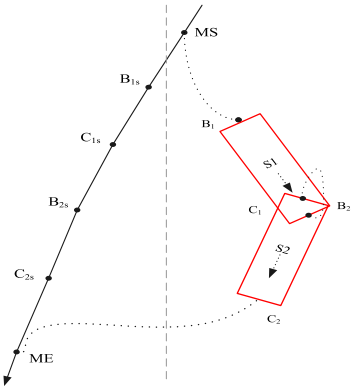

FIGURE 1. The schematic diagram of NGTI mission. MS-ME represents the sub-satellite line, B1-B2 and C1-C2 are the ground trajectories.

II. PROBLEM DESCRIPTION AND MODELLING

A. PROBLEM DESCRIPTION

Nonparallel-Ground-Track-Imaging is a dynamic and continuous imaging process oriented to the ground target. As shown in Fig 1, the trajectory of the ground trajectory is not parallel to the sub-satellite line which implies the satellite attitude should be adjusted in real time for tracking the trajectory.

Generally speaking, for an imaging mission, the ground trajectory is known and its start imaging time and terminate imaging time are also given, but the satellite attitude is unknown. Thus, the expect attitude should be firstly obtained according to the trajectory and the imaging time and then the satellite will be controlled to track the expected attitude subject to the external disturbance and the input saturation problem.

B. DYNAMIC MODEL OF SATELLITE

In this paper, the unit quaternion is suggested to describe the satellite attitude and for a rigid satellite, the nonlinear dynamic equation can be expressed as follows.

$$\begin{cases} \begin{bmatrix} \dot{\boldsymbol{q}} \\ \dot{q}_4 \end{bmatrix} = \frac{1}{2} \begin{bmatrix} q_4 \boldsymbol{I}_{3\times 3} + \boldsymbol{q}^{\times} & \boldsymbol{q} \\ -\boldsymbol{q}^{\mathrm{T}} & q_4 \end{bmatrix} \begin{bmatrix} \boldsymbol{\omega} \\ 0 \end{bmatrix} \\ \boldsymbol{J}\dot{\boldsymbol{\omega}} + \boldsymbol{\omega}^{\times}\boldsymbol{J}\boldsymbol{\omega} = \boldsymbol{u} + \boldsymbol{d} \end{cases} \tag{1}$$

where $\boldsymbol{q} = [q_1, q_2, q_3]^{\mathrm{T}}$ is the vector part of the quaternion and q_4 is the scalar part, $\boldsymbol{\omega} \in \boldsymbol{R}^{3\times 1}$ is the attitude angular rate, $\boldsymbol{J} \in \boldsymbol{R}^{3\times 3}$ is the moment of inertia, $\boldsymbol{u} \in \boldsymbol{R}^{3\times 1}$ is the control torque, $\boldsymbol{d} \in \boldsymbol{R}^{3\times 1}$ is the disturbance torque.

Remark 1. For any vector $\boldsymbol{v} \in \boldsymbol{R}^{3\times 1}$, $\boldsymbol{v}^{\times}$ denotes the skew symmetric matrix of $\boldsymbol{v}$, which can be expressed as

$$\boldsymbol{v}^{\times} = \begin{bmatrix} 0 & -v_3 & v_2 \\ v_3 & 0 & -v_1 \\ -v_2 & v_1 & 0 \end{bmatrix}$$

The attitude tracking errors are defined as

$$\begin{cases} \begin{bmatrix} \boldsymbol{q}_e \\ q_{e4} \end{bmatrix} = \begin{bmatrix} q_{d4}\boldsymbol{q} - \boldsymbol{q}^{\times} - q_4\boldsymbol{q}_d \\ \boldsymbol{q}_d^{\mathrm{T}}\boldsymbol{q} + q_4 q_{d4} \end{bmatrix} \\ \boldsymbol{\omega}_e = \boldsymbol{\omega} - \boldsymbol{C}_e\boldsymbol{\omega}_d \end{cases} \tag{2}$$

with

$$\boldsymbol{C}_e = (2q_{e4}^2 - 1)\boldsymbol{I}_{3\times 3} + 2\boldsymbol{q}_e\boldsymbol{q}_e^{\mathrm{T}} - 2q_{e4}\boldsymbol{q}_e^{\times}$$

where $\boldsymbol{q}_d$, q_{d4} and $\boldsymbol{\omega}_d$ are respectively the desired attitude quaternion and attitude angular rate.

For conveniently designing the control scheme, in this paper, we transform the attitude error dynamics of the satellite into an Eulerian-Lagrangian system as

$$\boldsymbol{M}(\boldsymbol{q}_e)\ddot{\boldsymbol{q}}_e + \boldsymbol{C}(\boldsymbol{q}_e, \dot{\boldsymbol{q}}_e)\dot{\boldsymbol{q}}_e + \boldsymbol{g}(\boldsymbol{q}_e) = \boldsymbol{G}^{-\mathrm{T}}(\boldsymbol{q}_e)(\boldsymbol{u} + \boldsymbol{d}) \tag{3}$$

with

$$\boldsymbol{G}(\boldsymbol{q}_e) = \frac{1}{2}(q_{e4}\boldsymbol{I}_{3\times 3} + \boldsymbol{q}_e^{\times}) \tag{4}$$

$$\boldsymbol{M}(\boldsymbol{q}_e) = \boldsymbol{G}^{-\mathrm{T}}\boldsymbol{J}\boldsymbol{G}^{-1} \tag{5}$$

$$\begin{aligned} \boldsymbol{C}(\boldsymbol{q}_e, \dot{\boldsymbol{q}}_e) = & -\boldsymbol{G}^{-\mathrm{T}}[(\boldsymbol{J}\boldsymbol{G}^{-1}\dot{\boldsymbol{q}}_e)^{\times} + (\boldsymbol{J}\boldsymbol{G}^{-1}\dot{\boldsymbol{q}}_e)^{\times}]\boldsymbol{G}^{-1} \\ & - \boldsymbol{G}^{-\mathrm{T}}[\boldsymbol{J}\boldsymbol{G}^{-1}\dot{\boldsymbol{G}} + (\boldsymbol{J}\boldsymbol{C}_e\boldsymbol{\omega}_d)^{\times}]\boldsymbol{G}^{-1} \\ & - \boldsymbol{G}^{-\mathrm{T}}[\boldsymbol{J}(\boldsymbol{C}_e\boldsymbol{\omega}_d)^{\times} + (\boldsymbol{C}_e\boldsymbol{\omega}_d)^{\times}\boldsymbol{J}]\boldsymbol{G}^{-1} \end{aligned} \tag{6}$$

$$\boldsymbol{g}(\boldsymbol{q}_e) = (\boldsymbol{C}_e\boldsymbol{\omega}_d)^{\times}\boldsymbol{J}\boldsymbol{C}_e\boldsymbol{\omega}_d + \boldsymbol{J}\boldsymbol{C}_e\dot{\boldsymbol{\omega}}_d \tag{7}$$

System (3) satisfies some properties [30], which are given as follows:

Property 1: For any $\boldsymbol{x} \in \boldsymbol{R}^{3\times 1}$, $\dot{\boldsymbol{M}}(\boldsymbol{q}_e) - 2\boldsymbol{C}(\boldsymbol{q}_e, \dot{\boldsymbol{q}}_e)$ is a skew symmetric matrix, that is, we can obtain

$$\boldsymbol{x}^{\mathrm{T}}\left[\dot{\boldsymbol{M}}(\boldsymbol{q}_e) - 2\boldsymbol{C}(\boldsymbol{q}_e, \dot{\boldsymbol{q}}_e)\right]\boldsymbol{x} = 0 \tag{8}$$

Property 2: $\boldsymbol{M}(\boldsymbol{q}_e)$ is a symmetric positive definite matrix.

Property 3: There exists $g_0 > 0$ with satisfying

$$\left\|\boldsymbol{g}(\boldsymbol{q}_e)\right\| \leq g_0 \tag{9}$$

TABLE 1. Coordinate frames involved.

Mark	Name	Definition
i	Inertial frame	Its origin is located at the center of Earth, the X axis is in the equatorial plane and points to the vernal equinox, the Z axis points to the North Pole, and the Y axis is determined by right hand ruler.
e	Fixed frame	Its origin is located at the center of Earth, the X axis is in the equatorial plane and points to zero longitude, the Z axis points to the North Pole, and the Y axis is determined by right hand ruler.
o	Orbital frame	Its origin is located at the center of satellite, the Z axis is along the negative position vector of the satellite, the Y axis is along the negative orbit normal and the X axis is determined by right hand ruler.
b	Body frame	Its three axes are respectively along the axes of inertia and the satellite attitude is defined as zero when it overlaps the orbital frame

III. SATELLITE ATTITUDE ADJUSTMENT STRATEGY

In this section, a mapping function between the satellite attitude and the ground trajectory will be firstly established. Different from [4], a space vector method is attempted to build this function, and then, we further proposed an attitude adjustment strategy via constant scanning velocity. In view of the vectors having different representations in different coordinate frames, hence, they should be unified to the same frame for operation. In this paper, we use the corner marks i, e, o and b to distinguish the involved coordinate frames, which are shown as TAB 1.

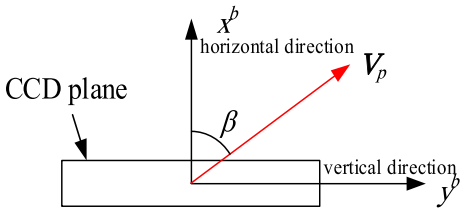

FIGURE 2. The schematic diagram of the CCD plane. The CCD camera is installed at the satellite barycenter with its boresight vector being along the z-axis of the *b*-frame, the horizontal direction of the CCD plane being along the x-axis and the vertical direction of the CCD plane being along the y-axis of b-frame.

A. IMAGE-MOTION VELOCITY AND DRIFT ANGLE DEFINITION

Ahead of anything else, the concepts of image-motion velocity and drift angle should be introduced. As shown in Fig 2, image-motion velocity refers to the projection of the scanning velocity for the ground trajectory onto the CCD plane. The drift angle refers to the included angle between the image-motion velocity vector and the horizontal direction of the linear array CCD, that is, the x^b-axis. Drift angle is an important factor that affects the imaging quality. Usually, it is expected to be zero.

In this section, we define the image-motion velocity vector onto the CCD plane as $\boldsymbol{V}_p = [\, v_{px} \;\; v_{py} \,]^{\mathrm{T}}$, thus, the drift angle can be expressed as

$$\beta = \arctan\left(\frac{v_{py}}{v_{px}}\right) \tag{10}$$

Obviously, the image motion is related to the dynamic scanning for the ground trajectory, in another word, the image-motion velocity is caused by the scanning velocity of the camera. We define $\boldsymbol{V}_T$ as the instantaneous scanning velocity vector According to the above concept, we have

$$\boldsymbol{V}_p = -\frac{f}{l}\left[\, \boldsymbol{V}_T^b(1) \quad \boldsymbol{V}_T^b(2) \,\right]^{\mathrm{T}} \tag{11}$$

where f denotes the focal distance of the camera, l is the distance from satellite to the ground point. $\boldsymbol{V}_T^b$ is the representation of $\boldsymbol{V}_T$ under b-frame.

B. THE MAPPING RELATIONSHIP BETWEEN THE GROUND TARGET AND THE SATELLITE ATTITUDE

In this section, we will deduce the satellite attitude while the camera's boresight pointing to a specified ground target instantaneously.

Property 4: $\boldsymbol{r}^{\alpha}$ and $\boldsymbol{r}^{\beta}$ are respectively the position vectors in α-frame and β-frame, $\boldsymbol{C}_{\alpha}^{\beta}$ denotes the direction cosine matrix from α-frame to β-frame and $\boldsymbol{\omega}_{\alpha\beta}$ denotes the rotational angular rate of β-frame around α-frame, the following equations as (12)-(15) are found.

$$\boldsymbol{C}_{\beta}^{\alpha} = \left(\boldsymbol{C}_{\alpha}^{\beta}\right)^{-1} = \left(\boldsymbol{C}_{\beta}^{\alpha}\right)^{\mathrm{T}}, \quad \left\|\boldsymbol{C}_{\beta}^{\alpha}\boldsymbol{r}^{\beta}\right\| = \left\|\boldsymbol{r}^{\beta}\right\| \tag{12}$$

$$\boldsymbol{r}^{\beta} = \boldsymbol{C}_{\alpha}^{\beta}\boldsymbol{r}^{\alpha} \tag{13}$$

$$\dot{\boldsymbol{r}}^{\beta} = \boldsymbol{C}_{\alpha}^{\beta}\dot{\boldsymbol{r}}^{\alpha} - [\boldsymbol{\omega}_{\alpha\beta}^{\beta}]^{\times}\boldsymbol{r}^{\beta} \tag{14}$$

$$\begin{aligned}\ddot{\boldsymbol{r}}^{\beta} = {} & \boldsymbol{C}_{\alpha}^{\beta}\ddot{\boldsymbol{r}}^{\alpha} - 2[\boldsymbol{\omega}_{\alpha\beta}^{\beta}]^{\times}\boldsymbol{C}_{\alpha}^{\beta}\dot{\boldsymbol{r}}^{\alpha} \\ & + 2\{[\boldsymbol{\omega}_{\alpha\beta}^{\beta}]^{\times}\}^2\boldsymbol{r}^{\beta} - [\dot{\boldsymbol{\omega}}_{\alpha\beta}^{\beta}]^{\times}\boldsymbol{r}^{\beta}\end{aligned} \tag{15}$$

As shown in Fig 3, the following geometry relationship should be satisfied

$$\boldsymbol{r}_{st}^{b} = \boldsymbol{C}_{e}^{b}\boldsymbol{r}_{et}^{e} - \boldsymbol{C}_{o}^{b}\boldsymbol{r}_{es}^{o} \Leftrightarrow \boldsymbol{r}_{st}^{e} = \boldsymbol{r}_{et}^{e} - \boldsymbol{C}_{o}^{e}\boldsymbol{r}_{es}^{o} \tag{16}$$

where $\boldsymbol{r}_{et}$ is the position vector of the ground point, $\boldsymbol{r}_{es}$ is the satellite position vector and $\boldsymbol{r}_{st}$ is the vector from the satellite to the ground point.

According to Eqs. (13)-(15), we can deduce that

$$\dot{\boldsymbol{r}}_{st}^{b} = -[\boldsymbol{\omega}_{eo}^{b}]^{\times}\boldsymbol{r}_{et}^{b} - [\boldsymbol{\omega}_{ob}^{b}]^{\times}\boldsymbol{r}_{st}^{b} + \boldsymbol{C}_{e}^{b}\dot{\boldsymbol{r}}_{et}^{e} - \boldsymbol{C}_{o}^{b}\dot{\boldsymbol{r}}_{es}^{o} \tag{17}$$

$$\begin{aligned}\ddot{\boldsymbol{r}}_{st}^{b} = {} & -2[\boldsymbol{\omega}_{eb}^{b}]^{\times}(\boldsymbol{C}_{e}^{b}\dot{\boldsymbol{r}}_{et}^{e}) + 2\{[\boldsymbol{\omega}_{eb}^{b}]^{\times}\}^2(\boldsymbol{C}_{e}^{b}\boldsymbol{r}_{et}^{e}) \\ & + 2[\boldsymbol{\omega}_{ob}^{b}]^{\times}(\boldsymbol{C}_{o}^{b}\dot{\boldsymbol{r}}_{es}^{o}) - 2\{[\boldsymbol{\omega}_{ob}^{b}]^{\times}\}^2(\boldsymbol{C}_{o}^{b}\boldsymbol{r}_{es}^{o}) \\ & + (\boldsymbol{C}_{e}^{b}\ddot{\boldsymbol{r}}_{et}^{e} - \boldsymbol{C}_{o}^{b}\ddot{\boldsymbol{r}}_{es}^{o}) - [\dot{\boldsymbol{\omega}}_{eo}^{b}]^{\times}\boldsymbol{r}_{et}^{b} - [\dot{\boldsymbol{\omega}}_{ob}^{b}]^{\times}r_{st}^{b}\end{aligned} \tag{18}$$

Usually, for ensuring the boresight points to the ground target and the drift angle being kept to be zero, thus, define the orthonormal vectors $\boldsymbol{e}_x, \boldsymbol{e}_y, \boldsymbol{e}_z$ with satisfying

$$\boldsymbol{e}_z = \frac{\boldsymbol{r}_{st}^{e}}{l}, \quad \boldsymbol{e}_y = \frac{\boldsymbol{r}_{st}^{e} \times \boldsymbol{V}_T^{e}}{\left\|\boldsymbol{r}_{st}^{e} \times \boldsymbol{V}_T^{e}\right\|}, \quad \boldsymbol{e}_x = \frac{\boldsymbol{e}_y \times \boldsymbol{e}_z}{\left\|\boldsymbol{e}_y \times \boldsymbol{e}_z\right\|} \tag{19}$$

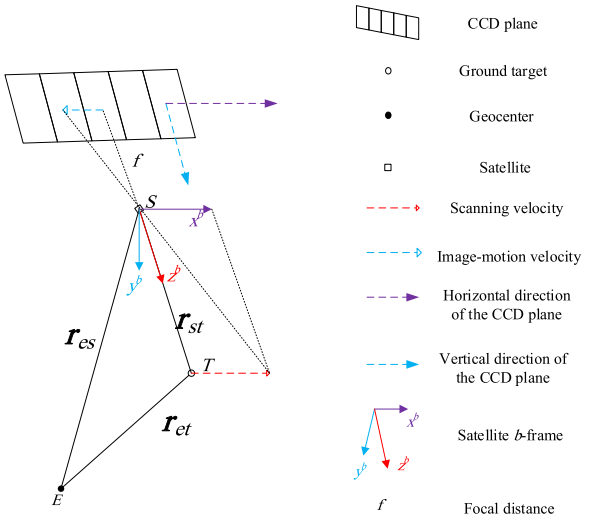

FIGURE 3. The schematic diagram of the space vectors. *E* is the center of Earth, *S* is the barycenter of satellite and *T* is the ground target pointed by the boresight vector of the camera.

where $\boldsymbol{e}_z$ ensures the boresight points to the ground point, $\boldsymbol{e}_y$ ensures the drift angle being zero and $\boldsymbol{e}_x$ satisfies the right hand principle. Thus, the following equation will be found.

$$\begin{aligned}\boldsymbol{I}_{3\times3} &= \boldsymbol{C}_{o}^{b}\boldsymbol{C}_{i}^{o}\boldsymbol{C}_{e}^{i}[\,\boldsymbol{e}_x \quad \boldsymbol{e}_y \quad \boldsymbol{e}_z\,] \\ \Rightarrow \boldsymbol{C}_{o}^{b} &= [\,\boldsymbol{e}_x \quad \boldsymbol{e}_y \quad \boldsymbol{e}_z\,]^{\mathrm{T}}\boldsymbol{C}_{i}^{e}\boldsymbol{C}_{o}^{i}\end{aligned} \tag{20}$$

According to the description of TABLE 2, it is easy to obtain the following representations of the vectors.

$$\begin{aligned}\boldsymbol{r}_{es}^{o} &= [\,0 \quad 0 \quad -r\,]^{\mathrm{T}}, \quad \boldsymbol{r}_{st}^{b} = [\,0 \quad 0 \quad l\,]^{\mathrm{T}} \\ \boldsymbol{\omega}_{io}^{o} &= [\,0 \quad -\omega_o \quad 0\,]^{\mathrm{T}}, \quad \boldsymbol{\omega}_{ie}^{e} = [\,0 \quad 0 \quad \omega_{ie}\,]^{\mathrm{T}}\end{aligned}$$

where r is the distance for the center of Earth to the satellite, ω_o is the orbital angular rate and ω_{ie} is the rotation angular rate of Earth.

With Eq. (16), we also can deduce that

$$l = \left\|\boldsymbol{r}_{st}^{b}\right\| = \sqrt{\left\|\boldsymbol{r}_{et}^{e}\right\|^2 + \left\|\boldsymbol{r}_{es}^{o}\right\|^2 - 2(\boldsymbol{r}_{es}^{o})^{\mathrm{T}}\boldsymbol{C}_{e}^{o}\boldsymbol{r}_{et}^{e}} \tag{21}$$

$\boldsymbol{C}_{i}^{e}$ and $\boldsymbol{C}_{o}^{i}$ can be determined by using Eqs. (22)-(23).

$$\boldsymbol{C}_{i}^{e} = \begin{bmatrix} c_G & s_G & 0 \\ -s_G & c_G & 0 \\ 0 & 0 & 1 \end{bmatrix} \tag{22}$$

$$\boldsymbol{C}_{o}^{i} = \begin{bmatrix} s_\theta & 0 & c_\theta \\ 0 & 1 & 0 \\ -c_\theta & 0 & s_\theta \end{bmatrix}\begin{bmatrix} 1 & 0 & 0 \\ 0 & s_i & -c_i \\ 0 & c_i & s_i \end{bmatrix}\begin{bmatrix} c_\Omega & s_\Omega & 0 \\ -s_\Omega & c_\Omega & 0 \\ 0 & 0 & 1 \end{bmatrix} \tag{23}$$

where G is the true sidereal hour angle, θ is the orbital latitude argument, i is the orbital inclination and Ω is the RAAN. The symbol c denotes *cos* and s denotes *sin*.

Then, we will deduce the expression of $\boldsymbol{\omega}_{ob}^{b}$.Firstly, with the constraint $\beta = 0$, that is, $\boldsymbol{V}_T^b(2) = 0$. Let

$$\boldsymbol{V}_T^{e} = \dot{\boldsymbol{r}}_{et}^{e}, \quad \boldsymbol{A}_T^{e} = \ddot{\boldsymbol{r}}_{et}^{e}, \quad d\boldsymbol{A}_T^{e} = \dddot{\boldsymbol{r}}_{et}^{e}$$

thereby the first and second components of $\boldsymbol{\omega}_{ob}^{b}$ can be determined by using Eqs. (17), (20) and (21).

$$\begin{bmatrix} \boldsymbol{\omega}_{ob}^{b}(1) \\ \boldsymbol{\omega}_{ob}^{b}(2) \end{bmatrix} = \frac{1}{l}\begin{bmatrix} \boldsymbol{V}_1^{b}(2) + C_{13}r \\ \boldsymbol{V}_T^{b}(1) - \boldsymbol{V}_1^{b}(1) - C_{13}r \end{bmatrix} \tag{24}$$

where $C_{ij} = \boldsymbol{C}_o^b(i,j)$ and $\boldsymbol{V}_1$ is defined as $\boldsymbol{V}_1 = [\boldsymbol{\omega}_{eo}]^{\times}\boldsymbol{r}_{et}$.

Furthermore, because $\dot{\boldsymbol{V}}_T^{b}(2) = 0$ also holds, take the derivation of $\boldsymbol{V}_T^{b}$, we can deduce that

$$\begin{aligned} \dot{\boldsymbol{V}}_T^{b} &= \boldsymbol{C}_e^{b}\boldsymbol{A}_T^{e} - [\boldsymbol{\omega}_{eb}^{b}]^{\times}\boldsymbol{V}_T^{b} \\ \Rightarrow \boldsymbol{\omega}_{ob}^{b}(3) &= \frac{\boldsymbol{A}_T^{b}(1) - \boldsymbol{A}_1^{b}(2) + \boldsymbol{\omega}_{ob}^{b}(1)\,\boldsymbol{V}_T^{b}(3)}{\boldsymbol{V}_T^{b}(1)} \end{aligned} \tag{25}$$

where $\boldsymbol{A}_1$ is defined as $\boldsymbol{A}_1 = [\boldsymbol{\omega}_{eo}]^{\times}\boldsymbol{V}_T$.

$\dot{\boldsymbol{\omega}}_{ob}^{b}$ also can be obtained with the similarly way, which is expressed as follows.

$$\dot{\boldsymbol{\omega}}_{ob}^{b} = \begin{bmatrix} -\dfrac{\boldsymbol{A}_2^{b}(2) + \boldsymbol{A}_3^{b}(2) + \boldsymbol{A}_T^{b}(2)}{l} \\ \dfrac{\boldsymbol{A}_2^{b}(1) + \boldsymbol{A}_3^{b}(1) + \boldsymbol{A}_T^{b}(1)}{l} \\ \dfrac{d\boldsymbol{A}_T^{b}(2) + \dot{\boldsymbol{\omega}}_{ob}^{b}(1)\,\boldsymbol{V}_T^{b}(3) + \boldsymbol{\chi}_1^{b}(2) - \boldsymbol{\chi}_2^{b}(2)}{\boldsymbol{V}_T^{b}(1)} \end{bmatrix} \tag{26}$$

with

$$\begin{aligned} \boldsymbol{A}_2 &= 2\{[\boldsymbol{\omega}_{eb}]^{\times}\}^2\boldsymbol{r}_{et} - 2[\boldsymbol{\omega}_{eb}]^{\times}\boldsymbol{V}_T \\ \boldsymbol{A}_3 &= -2\frac{\dot{r}}{r}[\boldsymbol{\omega}_{ob}]^{\times}\boldsymbol{r}_{es} - 2\{[\boldsymbol{\omega}_{ob}]^{\times}\}^2\boldsymbol{r}_{es} \\ \boldsymbol{\chi}_1 &= -2[\boldsymbol{\omega}_{eb}]^{\times}A_T + 2\{[\boldsymbol{\omega}_{eb}]^{\times}\}^2\boldsymbol{V}_T \\ \boldsymbol{\chi}_2 &= [\boldsymbol{\omega}_{io}\times\boldsymbol{\omega}_{ie} + \boldsymbol{\omega}_{ob}\times\boldsymbol{\omega}_{ie} + \boldsymbol{\omega}_{io}\times\boldsymbol{\omega}_{ob}]^{\times}\boldsymbol{V}_T \end{aligned}$$

Remark 2: It is worth to note that, $\dot{\omega}_o$ and $\ddot{r}$ are regard as constants, so that, $\dot{\boldsymbol{\omega}}_{ob}^{b}$ can be deduced as Eq. (26). Because the values of $r, \omega_o, G, \theta, i, \Omega$ can be determined if the moment t is given, thus, $\boldsymbol{C}_o^{b}$, $\boldsymbol{\omega}_{ob}^{b}$ and $\dot{\boldsymbol{\omega}}_{ob}^{b}$ are the functions depend on $\boldsymbol{r}_{et}^{e}$, $\boldsymbol{V}_T^{e}$, $\boldsymbol{A}_T^{e}$ and $d\boldsymbol{A}_T^{e}$, which will be deduced in next section.

$$\begin{aligned} \boldsymbol{C}_b^{o}(t) &\rightarrow \boldsymbol{f} : \left(\boldsymbol{r}_{et}^{e}, \boldsymbol{V}_T^{e}, t\right) \\ \boldsymbol{\omega}_{ob}^{b}(t) &\rightarrow \boldsymbol{g} : \left(\boldsymbol{r}_{et}^{e}, \boldsymbol{V}_T^{e}, \boldsymbol{A}_T^{e}, t\right) \\ \dot{\boldsymbol{\omega}}_{ob}^{b}(t) &\rightarrow \boldsymbol{h} : \left(\boldsymbol{r}_{et}^{e}, \boldsymbol{V}_T^{e}, \boldsymbol{A}_T^{e}, d\boldsymbol{A}_T^{e}, t\right) \end{aligned} \tag{27}$$

Here, let $\boldsymbol{\omega}_d = \boldsymbol{\omega}_{ob}^{b}$, the desired satellite attitude can be obtained by using the following formulas.

$$\begin{aligned} q_{4d} &= \frac{1}{2}\sqrt{1 + \sum_{i=1}^{3} C_{ii}}, \quad \boldsymbol{q}_d = \frac{1}{4q_{4d}}\begin{bmatrix} C_{23} - C_{32} \\ C_{31} - C_{13} \\ C_{12} - C_{23} \end{bmatrix} \\ \dot{\boldsymbol{q}}_d &= \boldsymbol{G}\left(\boldsymbol{q}_d\right)\boldsymbol{\omega}_d, \quad \dot{q}_{4d} = -\frac{1}{2}\dot{\boldsymbol{q}}_d^{\mathrm{T}}\boldsymbol{\omega}_d \\ \ddot{\boldsymbol{q}}_d &= \boldsymbol{G}\left(\boldsymbol{q}_d\right)\dot{\boldsymbol{\omega}}_d + \boldsymbol{G}\left(\dot{\boldsymbol{q}}_d\right)\boldsymbol{\omega}_d \\ \ddot{q}_{4d} &= -\frac{1}{2}\ddot{\boldsymbol{q}}_d^{\mathrm{T}}\boldsymbol{\omega}_d - \frac{1}{2}\dot{\boldsymbol{q}}_d^{\mathrm{T}}\dot{\boldsymbol{\omega}}_d \end{aligned} \tag{28}$$

Remark 3: For validating the solved $\boldsymbol{q}_d$ and $\boldsymbol{\omega}_d$ satisfy the kinematic relation, we discretize $\boldsymbol{q}_d$ and fit it by using the following n-order polynomial

$$\bar{q}_{d,k} = \sum_{i=0}^{n} a_{ik}t^{i}, \quad k = 1, 2, 3, 4, n \geq 2$$

where the weights a_{ik} can be solved by using the polyfit function in Matlab. Take the derivation of $\bar{q}_{d,k}$ and we get

$$\dot{\bar{q}}_{d,k} = \sum_{i=1}^{n} i a_{ik}t^{i-1}$$

Define $\delta\dot{\boldsymbol{q}}_d$ as

$$\delta\dot{\boldsymbol{q}}_d = \dot{\bar{\boldsymbol{q}}}_d - \begin{bmatrix} \dot{\boldsymbol{q}}_d \\ \dot{q}_{4d} \end{bmatrix} \tag{29}$$

where $\delta\dot{\boldsymbol{q}}_d$ should be zeros in theory.

C. CONTINUOUS SATELLITE ATTITUDE ADJUSTMENT VIA CONSTANT SCANNING VELOCITY

In this section, for simplifying the model, we assume that the ground trajectory is a great circle route on the earth surface. The start and terminate imaging point are respectively defined as (L_1, B_1) and (L_2, B_2) where L and B denote the geographic longitude and latitude respectively. Define V_{scan} as the scanning velocity which is set as a constant in this paper. If the imaging interval $[t_1, t_2]$ has been known, for any $t \in [t_1, t_2]$, we have

$$\begin{cases} \left(\boldsymbol{r}_{et}^{e}\right)^{\mathrm{T}}\boldsymbol{\eta}_1 = R_e\cos[\dfrac{V_{scan}}{R_e}(t - t_1)] \\ \left(\boldsymbol{r}_{et}^{e}\right)^{\mathrm{T}}\dfrac{\boldsymbol{\eta}_1\times\boldsymbol{\eta}_2}{\|\boldsymbol{\eta}_1\times\boldsymbol{\eta}_2\|} = 0, \|\boldsymbol{r}_{et}^{e}\| = R_e \end{cases} \tag{30}$$

where $\boldsymbol{\eta}_{1,2} = [\, c_{L_{1,2}}c_{B_{1,2}} \;\; s_{L_{1,2}}c_{B_{1,2}} \;\; s_{B_{1,2}}\,]^{\mathrm{T}}$ and R_e is the earth radius.

By using Eq. (30), the values of $\boldsymbol{r}_{et}^{e}$ at t moment can be solved, and then, we also can obtain the scanning velocity vector and its derivation under e-frame at t moment, which are as follows

$$\begin{cases} \boldsymbol{V}_T^{e} = \dfrac{V_{scan}}{R_e}\boldsymbol{e}_{\varpi}\times\boldsymbol{r}_{et}^{e} \\ \boldsymbol{A}_T^{e} = -\left(\dfrac{V_{scan}}{R_e}\right)^2\boldsymbol{r}_{et}^{e} \\ d\boldsymbol{A}_T^{e} = -\left(\dfrac{V_{scan}}{R_e}\right)^2\boldsymbol{V}_T^{e} \end{cases} \tag{31}$$

Substitute Eq. (31) into Eqs. (20) and (24)-(26), the desired attitude trajectory can be finally solved.

IV. THE TRACKING CONTROLLER DESIGN

In this section, a feedback tracking control scheme is designed to track the desired attitude.

A. PRELIMINARIES

Definition 1: $\forall \boldsymbol{x} \in \boldsymbol{R}^{n\times 1}$, we define

$$\mathbf{sig}^{\alpha}(\boldsymbol{x}) = [sign(x_1)\,|x_1|^{\alpha}, \cdots, \mathrm{sign}(x_n)\,|x_n|^{\alpha}]^{\mathrm{T}} \tag{32}$$

$$\mathbf{sign}(\boldsymbol{x}) = [sign(x_1), \cdots, sign(x_n)]^{\mathrm{T}} \tag{33}$$

where sign(·) and tanh(·) are respectively defined as

$$\text{sign}(x_i) = \begin{cases} 1, & x_i > 0 \\ 0, & x_i = 0 \\ -1, & x_i < 0 \end{cases} \tag{34}$$

$$\tanh(x_i) = \frac{2e^{x_i} + 1}{2e^{x_i} - 1} \tag{35}$$

Lemma 1 ([31]): $\forall \xi \in R$ and $-\infty < \xi < \infty$, then,

$$-\frac{\pi}{2} < gd(\xi) < \frac{\pi}{2}$$

where $gd(\xi)$ is the Gudermannian equation with following expression

$$gd(\xi) = \int_0^{\xi} \frac{1}{\cosh(\upsilon)} d\upsilon \tag{36}$$

Lemma 2 ([32]): Assume that $f(t) : [0, \infty) \to R$ is first-order continuously differentiable, if $\int_0^{+\infty} f(t)\, dt$ is existing and finite, then $\lim_{t\to\infty} f(t) = 0$.

Assumption 1: The external disturbance satisfies $\|\boldsymbol{d}\| \leq D$ and D is a known bounded constant.

Control Objective: The control objective in this paper can be described as: Given the desired trajectory $\boldsymbol{q}_d$, $\boldsymbol{\omega}_d$ and $\dot{\boldsymbol{\omega}}_d$, with *Assumption 1*, the system (1) can track them via a bounded control input, that is

$$\lim_{t\to\infty} (\boldsymbol{q}, q_4, \boldsymbol{\omega}) = \left(\boldsymbol{q}_d, q_{4d}, \boldsymbol{\omega}_d\right) \tag{37}$$

B. THE DISTURBANCE OBSERVER DESIGN

For improving the tracking accuracy, the disturbance torque should be dealt with reasonably. In this section, we consider that the disturbance torque is time-varying and a fixed-time disturbance observer is designed for estimating the disturbance torque.

With *Assumption 1*, the disturbance observer is designed as

$$\begin{cases} \boldsymbol{x} = \boldsymbol{\omega} + \boldsymbol{z} \\ \boldsymbol{J}\dot{\boldsymbol{z}} = \boldsymbol{\omega}^{\times}\boldsymbol{J}\boldsymbol{\omega} - \boldsymbol{u} - \boldsymbol{J}\boldsymbol{H}(\boldsymbol{x}) \end{cases} \tag{38}$$

with

$$\boldsymbol{H}(\boldsymbol{x}) = k_1 \mathbf{sign}(\boldsymbol{x}) + \frac{k_2}{2^{1-\eta}} \cosh\left(\frac{\boldsymbol{x}^{\mathrm{T}}\boldsymbol{x}}{2}\right)^{\eta} \mathbf{sig}^{1-2\eta}(\boldsymbol{x})$$

where $k_1 > \lambda_{\min}^{-1} D$, $\lambda_{\min}$ is the minimum eigenvalue of $\boldsymbol{J}$, $k_2 > 0$ and $0 < \eta < 0.5$.

Remark 4: For the term $\boldsymbol{H}(\boldsymbol{x})$, the variable $\boldsymbol{x}$ is an auxiliary variable and it has no physical meaning. The function $\boldsymbol{H}(\boldsymbol{x})$ is introduced to estimate the external disturbance and it is bounded with satisfying

$$\|\boldsymbol{H}(\boldsymbol{x})\| \leq \sqrt{3}\left(k_1 + \frac{k_2}{2^{1-\eta}}\right) \tag{39}$$

Theorem 1: Given the disturbance observer (38), the external disturbance torque $\boldsymbol{d}$ can be consistently estimated by the term $\boldsymbol{J}\boldsymbol{H}(\boldsymbol{x})$ within a fixed time T_2 which satisfies the following equation

$$T_2 = \frac{\pi}{2k_2\eta} \tag{40}$$

Proof: For proving *Theorem 1*, we select the following Lyapunov function

$$V_1 = \frac{1}{2}\boldsymbol{x}^{\mathrm{T}}\boldsymbol{x}$$

Obviously, Eq. (1) can be rewritten to following expression

$$\boldsymbol{u} = \boldsymbol{J}\dot{\boldsymbol{\omega}} + \boldsymbol{\omega}^{\times}\boldsymbol{J}\boldsymbol{\omega} - \boldsymbol{d} \tag{41}$$

Then, take the derivation of V_1 and in combination with Eqs. (38) and (41), we can obtain that

$$\begin{aligned} \dot{V}_1 &= \boldsymbol{x}^{\mathrm{T}}\dot{\boldsymbol{x}} \\ &= \boldsymbol{x}^{\mathrm{T}}(\dot{\boldsymbol{\omega}} + \dot{\boldsymbol{z}}) \\ &= \boldsymbol{x}^{\mathrm{T}}\boldsymbol{J}^{-1}\boldsymbol{d} - \boldsymbol{x}^{\mathrm{T}}\boldsymbol{H}(\boldsymbol{x}) \\ &= \boldsymbol{x}^{\mathrm{T}}\boldsymbol{J}^{-1}\boldsymbol{d} - k_1 \sum_{i=1}^{3} x_i \text{sign}(x_i) \\ &\quad - \frac{k_2}{2^{1-\eta}} \cosh\left(\frac{\boldsymbol{x}^{\mathrm{T}}\boldsymbol{x}}{2}\right)^{\eta} \sum_{i=1}^{3} x_i \text{sign}(x_i) |x_i|^{1-2\eta} \end{aligned} \tag{42}$$

According to *Assumption 1*, $\boldsymbol{J}^{-1}\boldsymbol{d} \leq \lambda_{\min}^{-1} D$ always holds, thus, Eq. (42) can be further deduced as

$$\begin{aligned} \dot{V}_1 &\leq \lambda_4^{-1} D \|\boldsymbol{x}\| - k_1 \|\boldsymbol{x}\| \\ &\quad - \frac{k_2}{2^{1-\eta}} \cosh\left(\frac{\boldsymbol{x}^{\mathrm{T}}\boldsymbol{x}}{2}\right)^{\eta} \sum_{i=1}^{3} x_i \text{sign}(x_i) |x_i|^{1-2\eta} \\ &= -\left(k_1 - \lambda_{\min}^{-1} D\right) \|\boldsymbol{x}\| - k_2 \cosh\left(V_1^{\eta}\right) V_1^{1-\eta} \\ &\leq -k_2 V_1^{1-\eta} \cosh\left(V_1^{\eta}\right) \\ &\leq 0 \end{aligned} \tag{43}$$

Eq. (43) can be rewritten into

$$\frac{dV_1}{\cosh\left(V_1^{\eta}\right) V_1^{1-\eta}} \leq -k_2 dt \tag{44}$$

Take the integration of Eq. (44), we obtain that

$$\int_0^{V_1^{\eta}(t)} \frac{1}{\cosh(\delta)} d\delta \leq -k_2\eta t + \int_0^{V_1^{\eta}(0)} \frac{1}{\cosh(\delta)} d\delta \tag{45}$$

From Eq. (43), we know that the Lyapunov function V_1 is monotonically decreasing, that is,

$$\int_0^{V_1^{\eta}(t)} \frac{1}{\cosh(\delta)} d\delta = 0$$

when and only when

$$-k_2\eta t + \int_0^{V_1^{\eta}(0)} \frac{1}{\cosh(\delta)} d\delta = 0$$

Thus, the state variable $\boldsymbol{x}$ will converge to a small region in T_1 and T_1 satisfies that

$$T_1 = \frac{1}{k_2\eta}\int_0^{V_1^{\eta}(0)} \frac{1}{\cosh(\delta)} d\delta \tag{46}$$

According to *Lemma 1*, we have $T_1 \leq (2k_2\eta)^{-1}\pi = T_2$, that is, the convergence time is independent of the initial values of the system states, which means the proposed observer (38) is fixed-time stable with

$$\lim_{t \geq T_2} \boldsymbol{d}(t) = \boldsymbol{JH}(\boldsymbol{x}) \tag{47}$$

Thus, *Theorem 1* has been proved.

C. THE TRACKING CONTROLLER DESIGN

In this section, a tracking controller will be designed for tracking the desired trajectory. Firstly, an integral sliding mode surface [30] is given as follows

$$\begin{aligned}\boldsymbol{S} = \dot{\boldsymbol{q}}_e &+ \int_0^t \boldsymbol{M}^{-1}(\boldsymbol{q}_e)\boldsymbol{C}(\boldsymbol{q}_e, \dot{\boldsymbol{q}}_e)\dot{\boldsymbol{e}}dt \\ &+ \int_0^t \boldsymbol{M}^{-1}(\boldsymbol{q}_e)[k_3\mathbf{tanh}(\lambda \boldsymbol{q}_e) + k_4\mathbf{tanh}(\lambda\dot{\boldsymbol{q}}_e)]dt\end{aligned} \tag{48}$$

where λ, k_3 and k_4 are positive constants.

With the sliding mode surface (48), an anti-saturation robust attitude tracking control scheme is given as follows

$$\begin{aligned}\boldsymbol{u} = &\boldsymbol{G}^{\mathrm{T}}(\boldsymbol{q}_e)\boldsymbol{g}(\boldsymbol{q}_e) - \boldsymbol{G}^{\mathrm{T}}(\boldsymbol{q}_e)[k_5\mathbf{sign}(\boldsymbol{M}^{-\mathrm{T}}(\boldsymbol{q}_e)\boldsymbol{S})] \\ &- \boldsymbol{G}^{\mathrm{T}}(\boldsymbol{q}_e)[k_3\mathbf{tanh}(\lambda \boldsymbol{q}_e) + k_4\mathbf{tanh}(\lambda\dot{\boldsymbol{e}})] - \hat{\boldsymbol{d}}\end{aligned} \tag{49}$$

where k_5 is positive constant and $\hat{\boldsymbol{d}} = \boldsymbol{JH}(\boldsymbol{x})$.

Remark 5: According to the conclusion of *Theorem 1*, $\boldsymbol{JH}(\boldsymbol{x})$ can track the external disturbance within a fixed time, hence, we introduce the term $\hat{\boldsymbol{d}}$ in the control scheme in the system (3) to estimate the external disturbance $\boldsymbol{d}$.

Theorem 2: For the system (1), under *Assumption 1*, the control objective (37) can be realized with the integral sliding mode surface (48) and the robust anti-saturation control scheme (49).

Proof: For proving *Theorem 2*, three steps i), ii) and iii) will be included and the proof process is given as follows.

i) Firstly, we validate the stability of $\boldsymbol{S}$. Here, the following Lyapunov function V_2 is selected.

$$V_2 = \frac{1}{2}\boldsymbol{S}^{\mathrm{T}}\boldsymbol{S}$$

According to Eq. (3), we can obtain that

$$\begin{aligned}\ddot{\boldsymbol{q}}_e = &-\boldsymbol{M}^{-1}(\boldsymbol{q}_e)\boldsymbol{C}(\boldsymbol{q}_e, \dot{\boldsymbol{q}}_e)\dot{\boldsymbol{q}}_e \\ &+ \boldsymbol{M}^{-1}(\boldsymbol{q}_e)\boldsymbol{G}^{-\mathrm{T}}(\boldsymbol{q}_e)(\boldsymbol{u}+\boldsymbol{d}) - \boldsymbol{M}^{-1}(\boldsymbol{q}_e)\boldsymbol{g}(\boldsymbol{q}_e)\end{aligned} \tag{50}$$

Take the derivation of V_2 and utilizing Eqs. (49)-(50), $\dot{V}_2$ can be deduced as follows.

$$\begin{aligned}\dot{V}_2 &= \boldsymbol{S}^{\mathrm{T}}\dot{\boldsymbol{S}} \\ &= \boldsymbol{S}^{\mathrm{T}}\ddot{\boldsymbol{q}}_e + \boldsymbol{S}^{\mathrm{T}}\boldsymbol{M}^{-1}\boldsymbol{C}\dot{\boldsymbol{q}}_e \\ &\quad + \boldsymbol{S}^{\mathrm{T}}\boldsymbol{M}^{-1}[k_3\mathbf{tanh}(\lambda \boldsymbol{q}_e) + k_4\mathbf{tanh}(\lambda\dot{\boldsymbol{q}}_e)] \\ &= -\boldsymbol{S}^{\mathrm{T}}\boldsymbol{M}^{-1}\boldsymbol{g} + \boldsymbol{S}^{\mathrm{T}}\boldsymbol{M}^{-1}\boldsymbol{G}^{-\mathrm{T}}(\boldsymbol{u}+\boldsymbol{d}) \\ &\quad + \boldsymbol{S}^{\mathrm{T}}\boldsymbol{M}^{-1}[k_3\mathbf{tanh}(\lambda \boldsymbol{q}_e) + k_4\mathbf{tanh}(\lambda\dot{\boldsymbol{q}}_e)] \\ &= -\boldsymbol{S}^{\mathrm{T}}\boldsymbol{M}^{-1}\boldsymbol{G}^{-\mathrm{T}}[\boldsymbol{d} - \boldsymbol{JH}(\boldsymbol{x})] \\ &\quad - \boldsymbol{S}^{\mathrm{T}}\boldsymbol{M}^{-1}[k_5\mathbf{sign}(\boldsymbol{M}^{-\mathrm{T}}\boldsymbol{S})]\end{aligned} \tag{51}$$

By using *Theorem 1*, $\boldsymbol{d} - \boldsymbol{JH}(\boldsymbol{x})$ can converge to zeros while $T \geq T_2$. On this basis, Eq. (51) can be further deduced as

$$\begin{aligned}\dot{V}_2 &= -k_5\boldsymbol{S}^{\mathrm{T}}\boldsymbol{M}^{-1}\mathbf{sign}(\boldsymbol{M}^{-\mathrm{T}}\boldsymbol{S}) \\ &= -k_5\sum_{i=1}^{2}[\boldsymbol{M}^{-1}\boldsymbol{S}^{\mathrm{T}}]_i \mathrm{sign}([\boldsymbol{M}^{-1}\boldsymbol{S}^{\mathrm{T}}]_i) \\ &= -k_5\left\|\boldsymbol{M}^{-1}\boldsymbol{S}^{\mathrm{T}}\right\| \\ &\leq 0\end{aligned} \tag{52}$$

Utilizing the Lyapunov stability criterion, step i) has been proved.

ii) Secondly, we validate that $\boldsymbol{q}_e$ and $\dot{\boldsymbol{q}}_e$ converge to zeros asymptotically. Define the following Lyapunov function

$$V_3 = \sum_{i=1}^{3}\int_0^{q_{ei}} k_3\tanh(\lambda q_{ei})dq_{ei} + \frac{1}{2}\dot{\boldsymbol{e}}^{\mathrm{T}}\boldsymbol{M}(\boldsymbol{q})\dot{\boldsymbol{q}}_e \tag{53}$$

Take the derivation of Eq. (53), we obtain that

$$\dot{V}_3 = \sum_{i=1}^{3} k_3\tanh(\lambda q_{ei})\dot{q}_{ei} + \frac{1}{2}\dot{\boldsymbol{q}}_e^{\mathrm{T}}\dot{\boldsymbol{M}}\dot{\boldsymbol{q}}_e + \dot{\boldsymbol{e}}^{\mathrm{T}}\boldsymbol{M}\ddot{\boldsymbol{q}}_e \tag{54}$$

With the conclusion of i), we can get $\boldsymbol{S}$ will converge to zeros asymptotically, that is, $\boldsymbol{S} \equiv 0$ always holds over time, which implies

$$\begin{aligned}\ddot{\boldsymbol{e}} = &-\boldsymbol{M}^{-1}\boldsymbol{C}(\boldsymbol{q}_e, \dot{\boldsymbol{q}}_e)\dot{\boldsymbol{q}}_e \\ &+ \boldsymbol{M}^{-1}[k_3\mathbf{tanh}(\lambda \boldsymbol{q}_e) + k_4\mathbf{tanh}(\lambda\dot{\boldsymbol{q}}_e)]\dot{\boldsymbol{q}}_e\end{aligned} \tag{55}$$

Substitute Eq. (55) into Eq. (54), we get

$$\begin{aligned}\dot{V}_3 = &\sum_{i=1}^{3} k_3\tanh(\lambda q_{ei})\dot{q}_{ei} \\ &+ \frac{1}{2}\dot{\boldsymbol{q}}_e^{\mathrm{T}}\dot{\boldsymbol{M}}\dot{\boldsymbol{q}}_e - \dot{\boldsymbol{q}}_e^{\mathrm{T}}\boldsymbol{C}\dot{\boldsymbol{q}}_e \\ &- \dot{\boldsymbol{q}}_e^{\mathrm{T}}[k_3\mathbf{tanh}(\lambda \boldsymbol{q}_e) + k_4\mathbf{tanh}(\lambda\dot{\boldsymbol{q}}_e)]\end{aligned} \tag{56}$$

By using *Properties 1*, Eq. (56) can be further deduced as

$$\begin{aligned}\dot{V}_3 &= \sum_{i=1}^{3} k_3\tanh(\lambda q_{ei})\dot{q}_{ei} - k_3\dot{\boldsymbol{q}}_e^{\mathrm{T}}\mathbf{tanh}(\lambda \boldsymbol{q}_e) \\ &\quad + \frac{1}{2}\dot{\boldsymbol{e}}^{\mathrm{T}}(\dot{\boldsymbol{M}} - 2\boldsymbol{C})\dot{\boldsymbol{e}} - \sum_{i=1}^{3} k_4\tanh(\lambda\dot{q}_{ei})\dot{q}_{ei} \\ &= -\sum_{i=1}^{3} k_4\tanh(\lambda\dot{q}_{ei})\dot{q}_{ei} \\ &\leq -k_4\left\|\dot{\boldsymbol{q}}_e\right\| \\ &\leq 0\end{aligned} \tag{57}$$

According to *Lemma 2*(Barbalat lemma), $\boldsymbol{q}_e$ and $\dot{\boldsymbol{q}}_e$ converge to zeros asymptotically.

With the constraint $\boldsymbol{q}_e^{\mathrm{T}}\boldsymbol{q}_e + q_{e4}^2 = 1$, we have $\lim_{t\to\infty} q_{e4} = 1$. According to the quaternion multiplication, we can get

$$\lim_{t\to\infty} (\boldsymbol{q}, q_4) = (\boldsymbol{q}_d, q_{4d}) \tag{58}$$

By using Eq. (2), we also can get

$$\lim_{t\to\infty} \boldsymbol{\omega} = \lim_{t\to\infty} [\boldsymbol{G}^{-1}(\boldsymbol{q}_e)\dot{\boldsymbol{q}}_e + \boldsymbol{C}_e\boldsymbol{\omega}_d] = \boldsymbol{\omega}_d \tag{59}$$

Thus, step ii) has been proved.

iii) Finally, we will analyze the saturation of $\boldsymbol{u}$. With the constraint $\boldsymbol{q}_e^{\mathrm{T}}\boldsymbol{q}_e + q_{e4}^2 = 1$, we know that $\|\boldsymbol{q}_e\| \le 1$, hence, we have

$$\|\boldsymbol{G}(\boldsymbol{q}_e)\| \le \frac{3}{2} \tag{60}$$

According to Eq. (39) and *Property 3*, it can be deduced that the control input $\boldsymbol{u}$ is bounded with satisfying

$$\begin{aligned}\|\boldsymbol{u}\| \le{}& \left\|\boldsymbol{G}^{\mathrm{T}}\right\| \|k_3\mathbf{tanh}(\lambda\boldsymbol{q}_e) + k_4\mathbf{tanh}(\lambda\dot{\boldsymbol{e}})\| \\ &+ \left\|\boldsymbol{G}^{\mathrm{T}}\right\| \left\|k_5\mathbf{sign}(\boldsymbol{M}^{-\mathrm{T}}\boldsymbol{S})\right\| + \|\boldsymbol{J}\boldsymbol{H}(\boldsymbol{x})\| + \left\|\boldsymbol{G}^{\mathrm{T}}\right\| \|\boldsymbol{g}\| \\ \le{}& \frac{3}{2}\sqrt{3}\sum_{i=3}^{5} k_i + \sqrt{3}\lambda_{\max}\left(k_1 + \frac{k_2}{2^{1-\eta}}\right) + \frac{3}{2}g_0 \end{aligned} \tag{61}$$

where $\lambda_{\max}$ is the maximum eigenvalue of $\boldsymbol{J}$. According to Eq. (7), we get

$$\begin{aligned}\|\boldsymbol{g}\| \le{}& \left\|(\boldsymbol{C}_e\boldsymbol{\omega}_d)^{\times}\boldsymbol{J}\boldsymbol{C}_e\boldsymbol{\omega}_d\right\| + \|\boldsymbol{J}\boldsymbol{C}_e\dot{\boldsymbol{\omega}}_d\| \\ \le{}& \lambda_{\max}\|\boldsymbol{\omega}_d\|_{\max}^2 + \lambda_{\max}\|\dot{\boldsymbol{\omega}}_d\|_{\max} = g_0 \end{aligned} \tag{62}$$

In this paper, $\boldsymbol{\omega}_d$ and $\dot{\boldsymbol{\omega}}_d$ is obviously bounded.

In conclusion, according to steps i) - iii), *Theorem 2* has been proved.

V. SIMULATION RESULTS

For validating the effectiveness of the proposed attitude adjustment strategy and the designed tracking controller, a numerical simulation will be carried on in this section.

TABLE 2. Initial parameters of the satellite orbit.

Symbol	Name	Value
T_0	Orbit Epoch	11 Jul 2019 04:00:00 UTCG
a	Semi major axis	7000 km
e	Eccentricity	0
inc	Inclination	28.5 deg
Ω	Argument of Perigee	0 deg
ω_0	RAAN	0 deg
f_0	True Anomaly	0 deg

A. SIMULATIONS FOR THE DESIRED TRAJECTORY

The simulation parameters are selected as TAB 2 and TAB 3. TAB 2 shows the initial orbit parameters and the observation mission is selected as the east coast of the United States, which is decomposed three line stripes as TAB 3. The imaging interval is also given in TAB 3. It should be noted that, t_1 and t_2 are relative to the Orbit Epoch. The initial instant of the simulation is set as $t_0 = 42168$s (11 Jul 2019 15:42:48 UTCG), which is 20.0s ahead of the beginning imaging time.

TABLE 3. Parameters of the stripes.

Stripe	(L_1, B_1)/deg	(L_2, B_2)/deg	$[t_1, t_2]$/s
S_1	(-76.48, 39.15)	(-76.69, 34.80)	[42188, 42288]
S_2	(-76.69, 34.80)	(-81.72, 30.79)	[42298, 42428]
S_3	(-81.72, 30.79)	(-80.00, 26.90)	[42438, 42530]

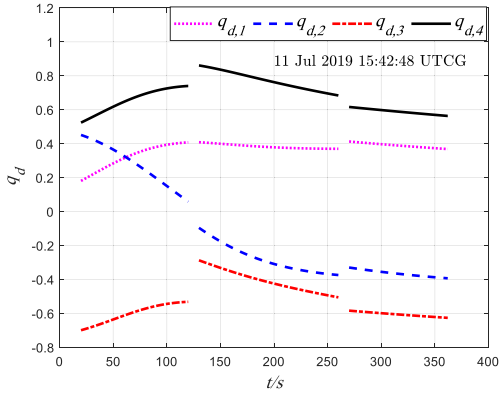

FIGURE 4. The curves of q_d from S_1 to S_3.

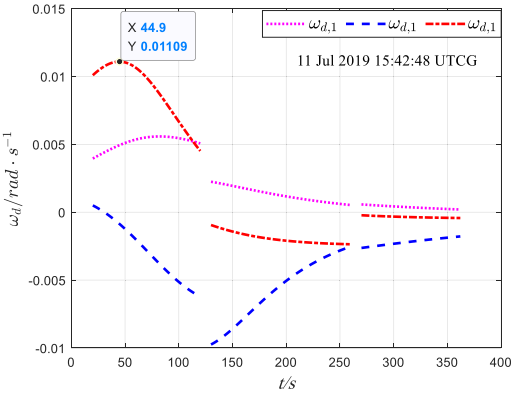

FIGURE 5. The curves of ω_d from S_1 to S_3.

The curves of $\boldsymbol{q}_d$, $\boldsymbol{\omega}_d$ and $\dot{\boldsymbol{\omega}}_d$ for the given stripes are presented in Figs 4-6.

For validating the solved desired trajectory satisfying the kinematic relation, the curves of $\delta\dot{\boldsymbol{q}}_d$ with Eq. (30) are given as Fig 7, from which we can see that the errors are respectively limited in about 6e-5, thus, it can be concluded that the solved desired trajectory satisfy the kinematic relation. That is to say, the attitude adjustment strategy proposed in Section III is mathematically rigorous. With similar method, we also can validate the kinematic relation between $\boldsymbol{\omega}_d$ and $\dot{\boldsymbol{\omega}}_d$.

B. SIMULATIONS FOR THE OBSERVER AND THE CONTROLLER

In this section, we will validate the disturbance observer (38) and the control scheme (48)-(49). Here, we select the stripe S_1 as the tracking object, the desired attitude can be

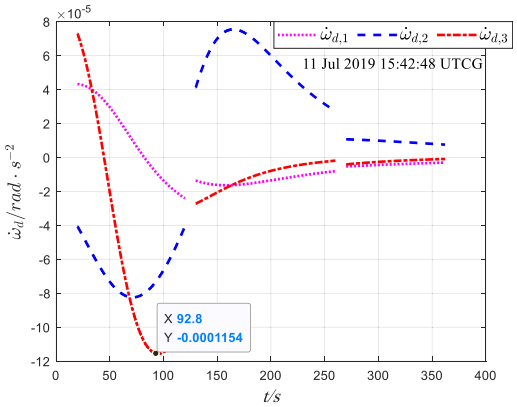

FIGURE 6. The curves of $\dot{\omega}_d$ from S_1 to S_3.

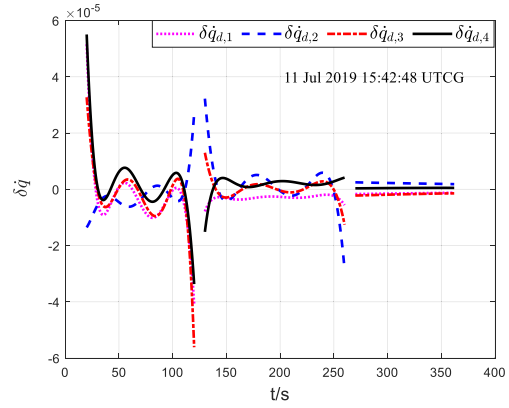

FIGURE 7. The curves of $\delta\dot{q}_d$ with Eq. (29).

expressed as

$$[\boldsymbol{q}_d, \boldsymbol{\omega}_d, \dot{\boldsymbol{\omega}}_d](\Delta t) = \begin{cases} [\boldsymbol{q}_d, \boldsymbol{\omega}_d, \dot{\boldsymbol{\omega}}_d](t_1), & t \in [t_0, t_1] \\ [\boldsymbol{q}_d, \boldsymbol{\omega}_d, \dot{\boldsymbol{\omega}}_d](t), & t \in (t_1, t_2] \end{cases}$$

where $\Delta t = t - t_0$. The satellite initial states are set as

$$\boldsymbol{q}(0) = [-0.3 \quad 0.2 \quad 0.3]^{\mathrm{T}}, \quad q_4(0) = 0.8832$$
$$\boldsymbol{\omega}(0) = \begin{bmatrix} 0.1 & 0 & -0.1 \end{bmatrix}^{\mathrm{T}} \text{ rad/s}$$

The satellite moment of inertia is set as

$$\boldsymbol{J} = diag(10, 8.5, 7.5)\text{kg} \cdot \text{m}^2$$

The disturbance torque is set as

$$\boldsymbol{d} = \begin{bmatrix} -0.2\sin(0.1\Delta t) \\ 0.2\sin(0.2\Delta t) \\ 0.5\sin(0.2\Delta t) \end{bmatrix} \text{N} \cdot \text{m}$$

The controller parameters are selected as

$$k_1 = 0.5,\ k_2 = 0.8,\ \eta = 0.3$$
$$k_3 = 3,\ k_4 = 2,\ k_5 = 0.2,\ \lambda = 100$$

Fig 8 shows the curves of the observed values for the disturbance torque, from which we can see that the disturbance torque can be tracked completely by the observer within about 1.7s. According to Eq. (40), we can calculate that $T_2 = 2.62\text{s} > 1.7\text{s}$. Hence, the proposed fixed-time

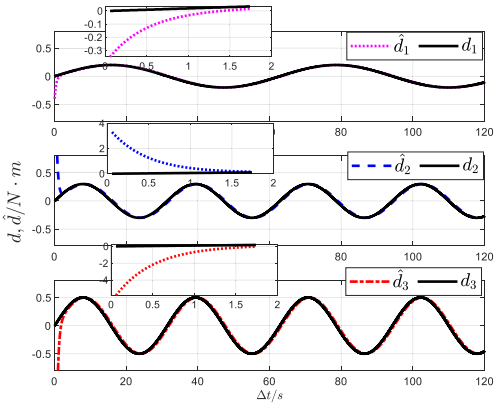

FIGURE 8. Observation of external disturbances with observer (38). $\hat{d}$ is the observed values for the disturbance torque.

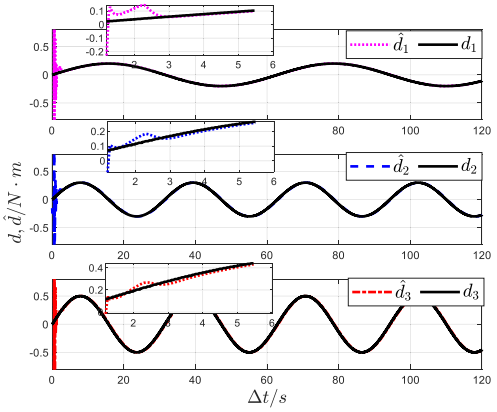

FIGURE 9. Observation of external disturbances with finite-time disturbance observer in [21].

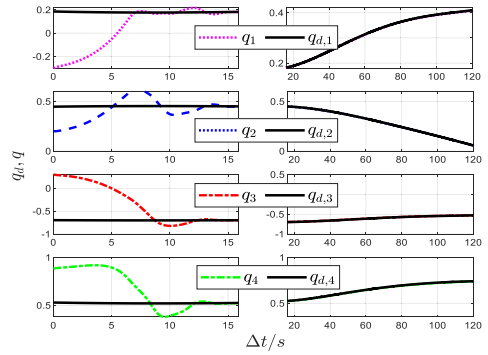

FIGURE 10. The curves of q and q_d.

disturbance observer is theoretically credible. For showing the superiority of the observer in this paper, we make a comparison with the disturbance observer proposed in [21], which is proved to be finite-time stable. The parameters of this observer are selected from [21] and the simulation result is shown in Fig 9, from which, we can see that it takes about 2.7s for the observer to track the external disturbance exactly. In addition, for achieving the observer's performance, 5 parameters are required to select and for the observer (38), merely 3 parameters are required, correspondingly.

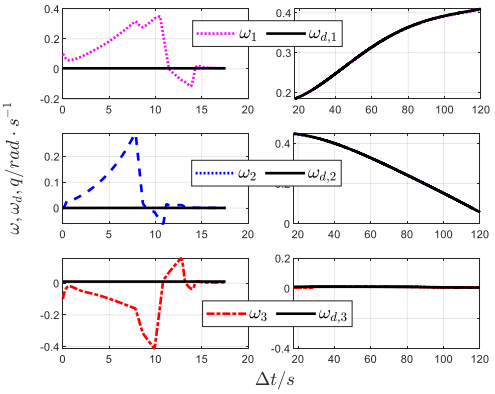

FIGURE 11. The curves of ω and ω_d.

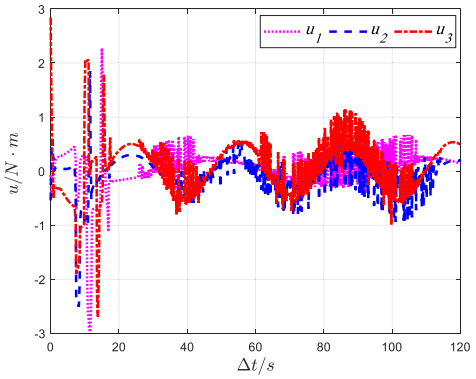

FIGURE 12. The curves of the control torque u.

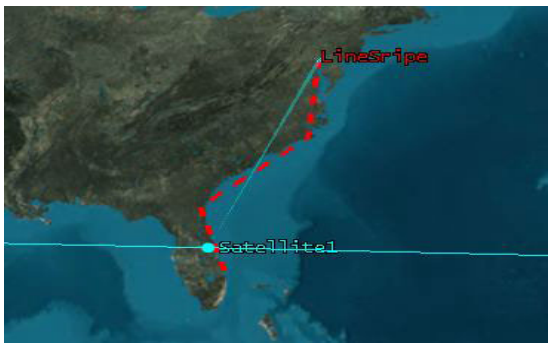

FIGURE 13. The desired trajectory presentation of the stripes in STK.

Figs. 10-11 respectively show the curves of $\boldsymbol{q}$ and ω, from which we can see that it takes about 15.8s for the satellite attitude tracking exactly the desired trajectory. That is to say, the attitude has been adjusted correctly before the satellite starting imaging for the ground target.

In addition, from Figs. 5-6, we can obtain that

$$\|\boldsymbol{\omega}_d\| \leq 0.01109\text{rad/s}, \quad \|\dot{\boldsymbol{\omega}}_d\| \leq 0.0001154\text{rad/s}^2$$

By using Eqs. (61)-(62), the upper boundary of the control torque is about $30.7\text{N} \cdot \text{m}$. The curves of the control torque is shown in Fig 12, from which we can see that the actual control torque is far less than the expected saturation boundary. Thus, we can conclude that the anti-saturation controller proposed in this paper is effective.

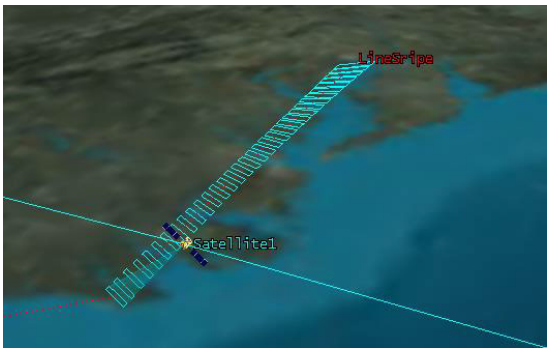

FIGURE 14. The scanning trajectory presentation for Stripe 1.

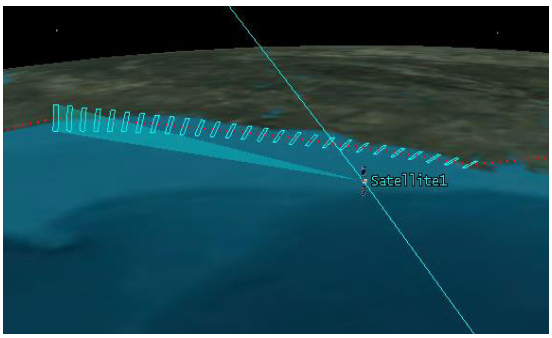

FIGURE 15. The scanning trajectory presentation for Stripe 2.

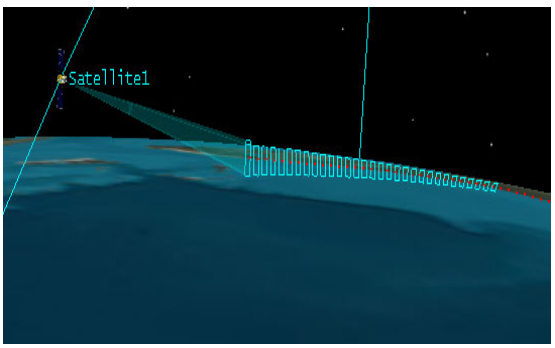

FIGURE 16. The scanning trajectory presentation for Stripe 3.

C. 3D GRAPHICS PRESENTATION WITH STK

For further validating the control algorithm, we utilize the System Tool Kit (STK) software to present the actual imaging effect, which are shown in Figs 13-16. Fig 13 shows the desired trajectory of the stripes in STK and Figs 14-16 are respectively the scanning trajectories for $S_1 \sim S_3$, from which we can see that:

i) The desired trajectories are coved well by the optical camera.

ii) The direction of the trajectories are roughly parallel to the horizontal direction of the CCD.

Thus, it can be concluded that the attitude adjustment strategy and the control scheme proposed in this paper are proved to be effective for the NGTI mission.

VI. CONCLUSION

Oriented to nonparallel-ground-track imaging of the agile optical satellite, an attitude adjustment strategy is proposed and a robust tracking controller subject to input saturation is designed in this paper. To be specific, the mapping function between the satellite attitude and the ground trajectory is firstly deduced by using space vector method. On this basis, an attitude adjustment strategy via constant scanning velocity is proposed, meanwhile, the drift angle of the camera can be eliminated with this strategy. Considering that the exact information of the external disturbance cannot be obtained and the input saturation problem, a fixed-time disturbance observer is designed based on the Gudermannian equation and then an anti-saturation robust control scheme via integral sliding mode is introduced. Finally, with the simulation analysis, the external disturbance can be quickly estimated by the disturbance observer and the desired attitude can be tracked exactly during the imaging process.

However, there also exists some shortcomings in this paper:

i) The stripes are rectilinear and the scanning velocity is constant in this paper. In fact, imaging mission could orient to a curvilinear stripe and the scanning velocity is not necessarily constant, which can be determined by using the nonlinear programming method according to the specified performance index. Due to limited space, this problem isn't discussed by this paper.

ii) In this paper, although the disturbance observer has been proved fixed-time stable, the tracking controller is asymptotically stable, which can be further improved in the future.

REFERENCES

[1] Y. Song, D. Huang, Z. Zhou, and Y. Chen, "An emergency task autonomous planning method of agile imaging satellite," *EURASIP J. Image Video Process.*, vol. 2018, no. 1, 2018, Art. no. 29.

[2] X. Wang, C. Han, R. Zhang, and Y. Gu, "Multiple agile earth observation satellites, oversubscribed targets scheduling using complex networks theory," 2018, *arXiv:1805.05053*. [Online]. Available: https://arxiv.org/abs/1805.05053

[3] L. He, X.-L. Liu, Y.-W. Chen, L.-N. Xing, and K. Liu, "Hierarchical scheduling for real-time agile satellite task scheduling in a dynamic environment," *Adv. Space Res.*, vol. 63, no. 2, pp. 897–912, 2019.

[4] D. Ye, Y. Tu, and Z. Sun, "Sliding mode control for nonparallelground-track imaging using Chebyshev neural network," *Acta Aeronaut. Astron. Sinica*, vol. 36, no. 9, pp. 3092–3104, 2015.

[5] Y. Wang, S. Tang, J. Guo, X. Wang, and C. Liu, "Fuzzy-logic-based fixed-time geometric backstepping control on SO(3) for spacecraft attitude tracking," *IEEE Trans. Aerosp. Electron. Syst.*, to be published.

[6] L. Zhao, J. Yu, and P. Shi, "Command filtered backstepping-based attitude containment control for spacecraft formation," *IEEE Trans. Syst., Man, Cybern., Syst.*, to be published.

[7] A.-M. Zou and K. D. Kumar, "Neural network-based distributed attitude coordination control for spacecraft formation flying with input saturation," *IEEE Trans. Neural Netw. Learn. Syst.*, vol. 23, no. 7, pp. 1155–1162, Jul. 2012.

[8] L. Zhao and Y. Jia, "Neural network-based distributed adaptive attitude synchronization control of spacecraft formation under modified fast terminal sliding mode," *Neurocomputing*, vol. 171, pp. 230–241, Jan. 2016.

[9] X. Cao, P. Shi, Z. Li, and M. Liu, "Neural-network-based adaptive backstepping control with application to spacecraft attitude regulation," *IEEE Trans. Neural Netw. Learn. Syst.*, vol. 29, no. 9, pp. 4303–4313, Sep. 2018.

[10] K. Lu, T. Li, and L. Zhang, "Active attitude fault-tolerant tracking control of flexible spacecraft via the Chebyshev neural network," *Trans. Inst. Meas. Control*, vol. 41, no. 4, pp. 925–933, 2019.

[11] N. Zhou, R. Chen, Y. Xia, J. Huang, and G. Wen, "Neural network–based reconfiguration control for spacecraft formation in obstacle environments," *Int. J. Robust Nonlinear Control*, vol. 28, no. 6, pp. 2442–2456, 2018.

[12] L.-G. Gong, Q. Wang, and C.-Y. Dong, "Spacecraft output feedback attitude control based on extended state observer and adaptive dynamic programming," *J. Franklin Inst.*, vol. 356, no. 10, pp. 4971–5000, 2019.

[13] L. Sun, "Adaptive fault-tolerant constrained control of cooperative spacecraft rendezvous and docking," *IEEE Trans. Ind. Electron.*, to be published.

[14] B. Wu, Q. Shen, and X. Cao, "Event-triggered attitude control of spacecraft," *Adv. Space Res.*, vol. 61, no. 3, pp. 927–934, 2018.

[15] Y. Liu, B. Jiang, J. Lu, J. Cao, and G. Lu, "Event-triggered sliding mode control for attitude stabilization of a rigid spacecraft," *IEEE Trans. Syst., Man, Cybern., Syst.*, to be published.

[16] C. Zhang, J. Wang, D. Zhang, and X. Shao, "Learning observer based and event-triggered control to spacecraft against actuator faults," *Aerosp. Sci. Technol.*, vol. 78, pp. 522–530, Jul. 2018.

[17] T. Chen and H. Wen, "Autonomous assembly with collision avoidance of a fleet of flexible spacecraft based on disturbance observer," *Acta Astron.*, vol. 147, pp. 86–96, Jun. 2018.

[18] D. Lee, "Nonlinear disturbance observer-based robust control for spacecraft formation flying," *Aerosp. Sci. Technol.*, vol. 76, pp. 82–90, May 2018.

[19] B. Guo and Y. Chen, "Adaptive fast sliding mode fault tolerant control integrated with disturbance observer for spacecraft attitude stabilization system," *ISA Trans.*, to be published.

[20] L. Sun, W. Huo, and Z. Jiao, "Disturbance-observer-based robust relative pose control for spacecraft rendezvous and proximity operations under input saturation," *IEEE Trans. Aerosp. Electron. Syst.*, vol. 54, no. 4, pp. 1605–1617, Aug. 2018.

[21] Q. Zong and S. Shao, "Decentralized finite-time attitude synchronization for multiple rigid spacecraft via a novel disturbance observer," *ISA Transactions*, vol. 65, pp. 150–163, Nov. 2016.

[22] Q. Lan, C. Qian, and S. Li, "Finite-time disturbance observer design and attitude tracking control of a rigid spacecraft," *J. Dyn. Syst., Meas., Control*, vol. 139, no. 6, 2017, Art. no. 061010.

[23] Q. Zong, X. Zhang, S. Shao, B. Tian, and W. Liu, "Disturbance observer-based fault-tolerant attitude tracking control for rigid spacecraft with finite-time convergence," *Proc. Inst. Mech. Eng., G, J. Aerosp. Eng.*, vol. 233, no. 2, pp. 616–628, 2019.

[24] A.-M. Zou, A. H. J. de Ruiter, and K. D. Kumar, "Disturbance observer-based attitude control for spacecraft with input MRS," *IEEE Trans. Aerosp. Electron. Syst.*, vol. 55, no. 1, pp. 384–396, Feb. 2019.

[25] B. Li, Q. Hu, Y. Yang, and O. A. Postolache, "Finite-time disturbance observer based integral sliding mode control for attitude stabilisation under actuator failure," *IET Control Theory Appl.*, vol. 13, no. 1, pp. 50–58, Jan. 2018.

[26] Z. Liu, J. Liu, and L. Wang, "Disturbance observer based attitude control for flexible spacecraft with input magnitude and rate constraints," *Aerosp. Sci. Technol.*, vol. 72, pp. 486–492, Jan. 2018.

[27] S. Cao and Y. Zhao, "Anti-disturbance fault-tolerant attitude control for satellites subject to multiple disturbances and actuator saturation," *Nonlinear Dyn.*, vol. 89, no. 4, pp. 2657–2667, 2017.

[28] Q. Hu, Y. Shi, and X. Shao, "Adaptive fault-tolerant attitude control for satellite reorientation under input saturation," *Aerosp. Sci. Technol.*, vol. 78, pp. 171–182, Jul. 2018.

[29] Y.-H. Li, X.-D. Wang, W.-G. Liu, and Z. Wang, "Analysis and reduction of the TDI CCD charge transfer image shift," *Appl. Opt.*, vol. 56, no. 33, pp. 9233–9240, 2017.

[30] Y. Guo, B. Huang, A.-J. Li, and C.-Q. Wang, "Integral sliding mode control for Euler-Lagrange systems with input saturation," *Int. J. Robust Nonlinear Control*, vol. 29, no. 4, pp. 1088–1100, 2019.

[31] A. Khanzadeh and M. Pourgholi, "Fixed-time sliding mode controller design for synchronization of complex dynamical networks," *Nonlinear Dyn.*, vol. 88, no. 4, pp. 2637–2649, Jun. 2017.
[32] S. Sastry and M. Bodson, *Adaptive Control: Stability, Convergence, and Robustness*. Upper Saddle River, NJ, USA: Prentice-Hall, 2011.

LIN ZHAO received the bachelor's degree from Harbin Engineering University, in 1989, and the Ph.D. degree in engineering from the Harbin Institute of Technology, in 1995. He is currently a Professor with Harbin Engineering University. His research interests include the navigation and positioning of GPS, BeiDou, path planning, and control and guidance of spacecraft.

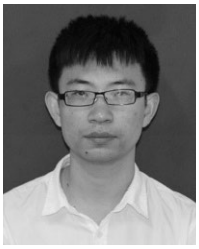

KUN ZHAO received the bachelor's degree from the Nanjing University of Aeronautics and Astronautics, in 2013. Since 2014, he has been a Doctor with the Automation College, Harbin Engineering University. His research interests include mission planning, optical control for agile satellite, and the distributed control for spacecraft formation.

YONG HAO received the bachelor's, master's, and Ph.D. degrees from Harbin Engineering University, in 2007, 2011, and 2016, respectively. He is currently a Lecturer with the Automation College, Harbin Engineering University. His research interests include mission planning and control for spacecraft.

XINYU ZHANG received the master's degree in engineering from the Computing College, Harbin Engineering University, in 2013, where he is currently pursuing the Ph.D. degree with the Automation College. His main research interests include spacecraft formation control and distributed systems.

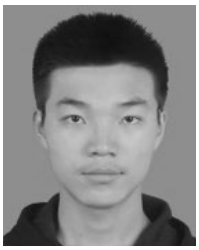

YUSHAN HE received the bachelor's degree from Zhengzhou University, in 2019. He is currently pursuing the master's degree with the Automation College, Harbin Engineering University. His research interest includes spacecraft formation attitude control.